Rip Current Prediction

Austin, Martin J.; Scott, Tim M.; Russell, Paul E.; Masselink, G.

Journal of Coastal Research

DOI:
10.2112/JCOASTRES-D-12-00093.1

Published: 01/10/2013

Version created as part of publication process; publisher's layout; not normally made publicly available

Journal of Coastal Research	00	0	000–000	~~West Palm Beach~~, Florida	Month 0000

Rip Current Prediction: Development, Validation, and Evaluation of an Operational Tool

Martin J. Austin, Tim M. Scott, Paul E. Russell, and Gerd Masselink

School of Marine Science and Engineering
Plymouth University
Drake Circus, Plymouth PL4 8AA, UK

www.cerf-jcr.org

www.JCRonline.org

ABSTRACT

Austin, M.J.; Scott, T.M.; Russell, P.E., and Masselink, G., 0000. Rip current prediction: development, validation, and evaluation of an operational tool. *Journal of Coastal Research,* 00(0), 000–000. ~~West Palm Beach~~ (Florida), ISSN 0749-0208.

This contribution details the development, validation, and evaluation of an operational rip current prediction tool. Field measurements of rip current dynamics from a macrotidal beach in the southwest U.K. collected over 87 tidal cycles indicate that the rip currents are highly dynamic over a range of temporal and spatial scales. The morphology of the lower intertidal beach face provides the primary spatial control of the rip currents, whereas the variation in the pattern of wave dissipation due to the tidal translation of the surf zone at spring-neap and semidiurnal frequencies is the principle temporal control. The Lagrangian drift pattern associated with the rip currents displays three key behaviors: rotation, alongshore, and exit. Rotation and exit are observed under moderate conditions, whereas strong alongshore-directed currents prevail during energetic conditions. An operational regional wave model is used to force a two-dimensional horizontal (2D-H) nonstationary model for coupled wave propagation and flow to predict the rip current speed and behavior. The model is calibrated using measured Eulerian field data, and the resultant circulation patterns are validated against measured Lagrangian data. The model was run for a 2-month hindcast period, and the flow speed and behavioral output were combined to allocate a rip current hazard rating. The model performance was evaluated against beach lifeguard incident statistics; 64% of recorded incidents occurred under predicted high-risk conditions, and 36% occurred during medium-risk conditions. The rip hazard prediction model was subsequently run in forecast mode to provide an example of operational-type output.

ADDITIONAL INDEX WORDS: *Macrotidal, XBeach, surf zone, drifter, modeling, hazard, tide, wave dissipation.*

INTRODUCTION

It is now well established that rip currents present the greatest natural hazard to beach users along wave-dominated coasts. In Australia and Florida alone, rip currents are responsible for 50 and 25 drownings each year, respectively (Lushine, 1991; Short and Hogan, 1994), whereas in the southwest of England, roughly two-thirds of all reported incidents (total number = 12,521 between 2006 and 2011) are due to rip currents (Scott *et al.*, 2011). Even in countries generally not associated with rip currents and a surf culture, rip currents are often the main beach hazard (Kim, Kim and Lee, 2011; Verbeek, 2011).

The behavior of rip currents and the risk they present to beach users are, to some degree, predictable and directly related to rip dynamics (MacMahan, Thornton, and Reniers, 2006). For example, intermediate sandy beaches, *i.e.*, beaches with bar morphology subjected to medium-energy wave conditions, are considered particularly conducive to rip current activity (Brander, 1999; Wright and Short, 1984). On tidal beaches, beach rip currents appear to be especially active around low tide, whether in micro- (McKenzie, 1958), meso- (Bruneau *et al.*, 2009), or macrotidal environments (Austin *et al.*, 2011). Swell waves also seem to present more hazardous rip current conditions than wind waves. As a result, rip risk prediction tools, based on wave/tide conditions and ideally including observations of beach morphology, can be developed at a regional scale to help identify and warn against hazardous rip conditions. Examples of such regional prediction tools include Lushine (1991) and Engle *et al.* (2002). Although such models can be fit for purpose, a frequent shortcoming is that, because of their regional perspective, they fail to include necessary site-specific factors such as beach state. Predictions therefore become over generalized and simplistic and are generally of limited use.

An alternative approach is to develop a site-specific rip risk prediction tool—ideally at a particularly busy and hazardous beach or stretch of coast to help justify the effort involved in developing such a tool. There are two published examples of such predictive tools, both at an experimental stage. Song and Bae (2011) developed forecasting tools for rip current generation based on a network of sensors and are in the process of formulating an automatic warning system for beach goers on Haeundae beach in South Korea. In the Netherlands, a rip current prediction model system is being piloted that is based on measured bathymetry and application of the XBeach hydrodynamic model (Roelvink *et al.*, 2009) to predict current

DOI: 10.2112/JCOASTRES-D-12-00093.1 received 16 May 2012; accepted in revision 30 June 2012.
martin.austin@plymouth.ac.uk
Published Pre-print online XX Month XXXX.

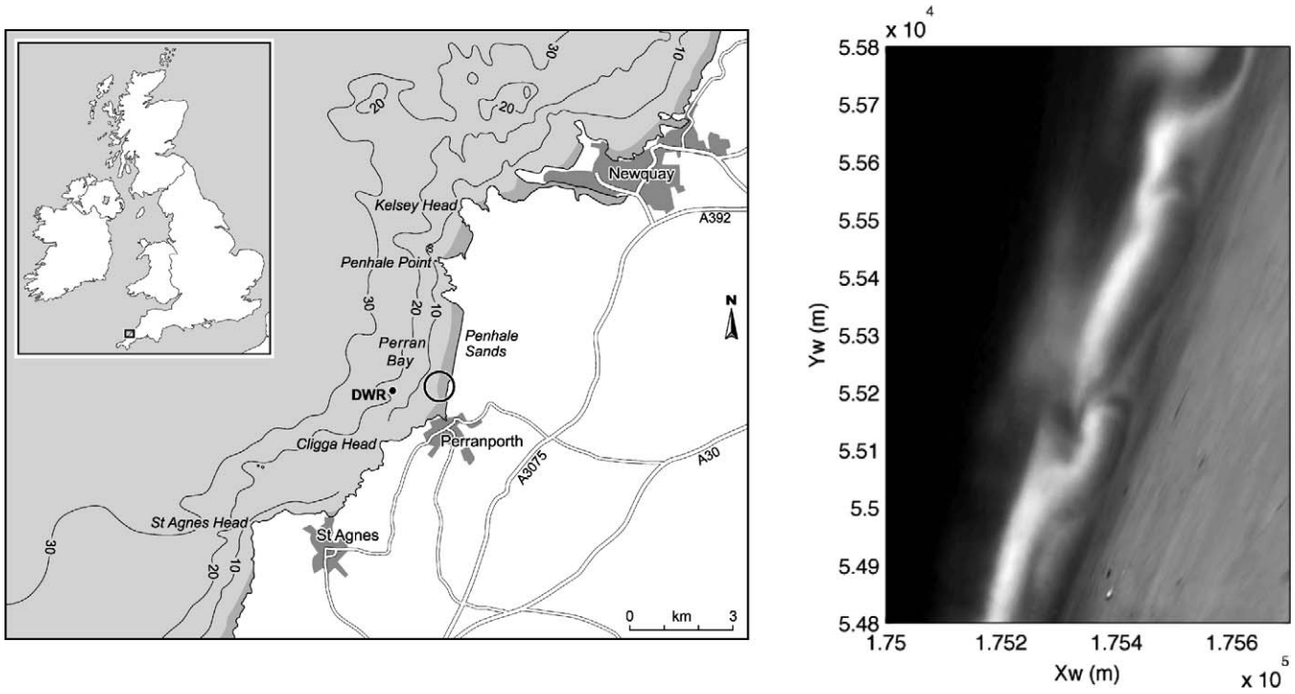

Figure 1. Overview of study area. (Left panel) Map of Perranporth (inset shows U.K. context). (Right panel) Merged and rectified ARGUS timex image of the low-tide bar/rip morphology. Coordinates are Ordnance Survey National Grid (OSTN02).

speeds and directions on Egmond beach (CoSMoS, 2012). The tool developed in the Netherlands is particularly useful in that it can be used to assess rip risk for different sections of the beach and for different times depending on the tidal elevation and wave conditions. Real-time forecasts are being issued and the predicted flow velocities are color-coded to highlight the speed of the nearshore currents. A significant shortcoming of these two rip risk prediction models is that there has been very limited comparison between field observations of flow velocities and model predictions. In addition, the rip risk predictions have not been compared with incidence (rescue) records, and it remains unclear whether the tool provides useful information.

The Dynamics of Rips and Implications for Beach Safety (DRIBS) project is a partnership between Plymouth University (PU) and the Royal National Lifeboat Institution (RNLI). From the project's inception, the RNLI have guided the overall objectives of DRIBS such that the scientific output informs the RNLI to help improve all aspects of the beach lifeguarding service, from beach risk assessment, lifeguard training, and resource deployment, to save lives. During the DRIBS project, two intensive periods of fieldwork in the spring (May–June; experiment D1) and autumn (October; experiment D2) of 2011 were carried out at Perranporth beach on the north Cornish coast in the U.K. The aim of these two experiments was to build a comprehensive database of rip current behavior and dynamics over a range of forcing conditions. To this end, data were collected using a combination of Eulerian *in situ* instruments, Lagrangian surf zone drifters, ARGUS remote video sensing, and bathymetric/topographic surveying.

In this paper, we present an operational rip risk prediction tool that is specific for Perranporth beach in the southwest of England. The model is based on the application of a hydrodynamic model, using measured bathymetry and measured or predicted wave conditions, to compute nearshore current speeds, which are then used to develop a real-time rip risk prediction tool. The objectives of this paper are to (1) discuss the key characteristics of the rip current dynamics at the study site using Lagrangian and Eulerian field data, (2) describe the different components of the modeling tool, (3) validate the output of the hydrodynamic model using field measurements, (4) evaluate performance of the tool with incident records, (5) illustrate the operational nature of the model, and (6) provide suggestions for further development of the tool. Although the rip risk prediction tool is site-specific, the overall approach followed here, comprising the different stages of rip current characterization using field observations, hydrodynamic model development and validation, and evaluation of the tool with beach rescue data, can be adopted to other environments characterized by rip currents.

DESCRIPTION OF STUDY AREA

Perranporth beach in the southwest of England is typical of the open-coast beaches found along the 160-km length of the northern coast of the peninsula (Figure 1). These beaches

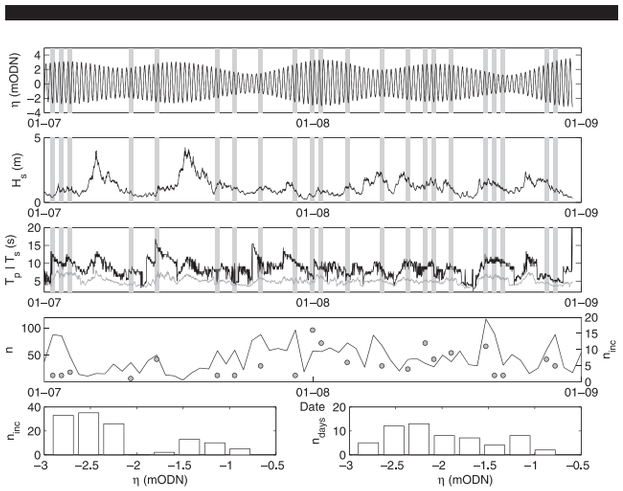

Figure 2. Summary of hydrodynamic conditions and incidents at Perranporth during July–August 2011. (Top to bottom) Tidal elevation η; significant wave height H_s; peak T_p (black) and mean T_s (gray) wave periods; average number of people in the water per hour n (line, left axis) and number of incidents n_{inc} (circle, right axis); histogram of number of incidents split into water level classes; and histogram of occurrence of daily minimum water level. Grey bands in the top three panels mark the occurrence of rescue incidents.

characteristically display low-gradient, sandy, sub- and intertidal zones backed by hard-rock cliffs or steep sand dunes. The southwest region is a renowned tourist location with 5 million visitors annually, and Perranporth is a notable tourist hotspot. It is common for Perranporth to have recorded in-water bather numbers exceeding 1000 during peak summer holiday periods.

Perranporth is a macrotidal beach with a semidiurnal tidal regime and a mean spring tide range of 6.3 m. It sits in the low-tide bar-rip (LTBR) beach state group of Masselink and Short (1993) and Scott *et al*. (2011), with a 400–500-m-wide intertidal zone, pronounced low-tide bar/rip morphology, and a subtidal bar (Figure 1), which vary over a range of timescales. The intertidal beach is relatively flat ($\tan\beta = 0.015 - 0.025$), and the beach is composed of medium quartz sand (median sediment size, $D_{50} = 0.28 - 0.34$ mm; median sediment fall velocity, $w_s = 0.03 - 0.04$ m s^{-1}). The beach faces west-northwest and receives a mixture of Atlantic swell (westerly waves) and locally generated wind waves (northerly waves); it has an annual average significant wave height and peak period of $H_s = 1.6$ m and $T_p = 10.5$ s, respectively, based on analysis of the Perranporth inshore directional wave rider buoy (DWR; refer to Figure 1 for location).

The hydrodynamic conditions, number of people in the water, and recorded incidents for Perranporth during July–August 2011 are shown in Figure 2. Since 2006, RNLI lifeguards have kept comprehensive records of all beach incidents occurring during patrol hours, as well as hourly logs of estimated numbers of beach users on land and in the sea. Incident metadata includes victim demographics and severity, as well as environmental causes, of incident (*i.e.*, rip currents, tidal cut-off, *etc*.). RNLI lifeguards at Perranporth respond to an average of 239 rip current–related incidents per year, of which 12 are considered lives saved. During the patrol season (April–October), there are on average 30 water users (50th percentile) at any one time (1000–1800 h) at Perranporth. Every year this number peaks at more than 2000 during the busiest days. The quantification of beach user numbers enables the normalization of incident numbers to exposure, giving a useful measure of risk (probability = number of incidents divided by number of beach users).

In Figure 2, several salient points are worth noting. A greater number of incidents are typically recorded during spring tides, periods of smaller waves and longer period (or transitions to longer period) waves. The best example of such convergence of hazardous conditions occurred at the start of August when, during two consecutive days, 15 and 12 people were rescued. The greater number of spring tide incidents are typically linked to the intertidal bar/rip morphology being accessible to bathers around low water. The increased probability of incidents under longer period small waves appears linked to swell waves maximizing rip flows and increased bather exposure to the surf zone and rip currents because of calm periods between well-developed wave groups (Scott *et al*., 2011).

DATA COLLECTION

Bathymetric and Topographic Surveying

The intertidal and subtidal beach morphology at Perranporth was surveyed at least every 2 weeks during field experiments D1 (spring deployment) and D2 (autumn field deployment) and every 4–6 weeks throughout 2011. A survey region of 1500 × 1500 m in the alongshore (Y_w) and cross-shore (X_w) directions was measured from the dune system to a water depth of ~16 m (Figure 3). Intertidal topography (dune foot to mean low water spring [MLWS] shoreline) was collected using a Trimble real-time kinematic (RTK) GPS system mounted on an all-terrain vehicle (ATV) during low-tide periods. Subtidal bathymetry was collected using RTK-GPS and a single-beam echo sounder mounted onto a personal water craft (PWC) during high tide. Bathymetric data were collected along regularly spaced cross-shore transects ($\Delta Y = 25$ m), which overlapped with the intertidal survey by approximately 100 m. The ATV and PWC survey datasets were subsequently merged together and interpolated onto a regular grid using the quadratic loess scale-controlled interpolation method (Plant, Holland, and Puleo, 2002). All positions are reported as real-world coordinates (X_w, Y_w) on the U.K. National Grid (OSTN02) and elevations are reduced to Ordnance Datum Newlyn (ODN).

Eulerian Data

In situ instrument rig arrays were deployed around the MLWS shoreline region to record water level, wave height, flow velocity, and suspended sediment concentration across the intertidal bar, feeder, and rip channels (Figure 3). Two instrument arrays were deployed during D1. The first was a cross-shore array of four rigs over the crest of the intertidal bar and landward trough (R1–R4), each mounting a pair of bidirectional miniature electromagnetic currents meters, a high-precision pressure transducer (PT), and an optical backscatter sensor (OBS). The second was an approximately

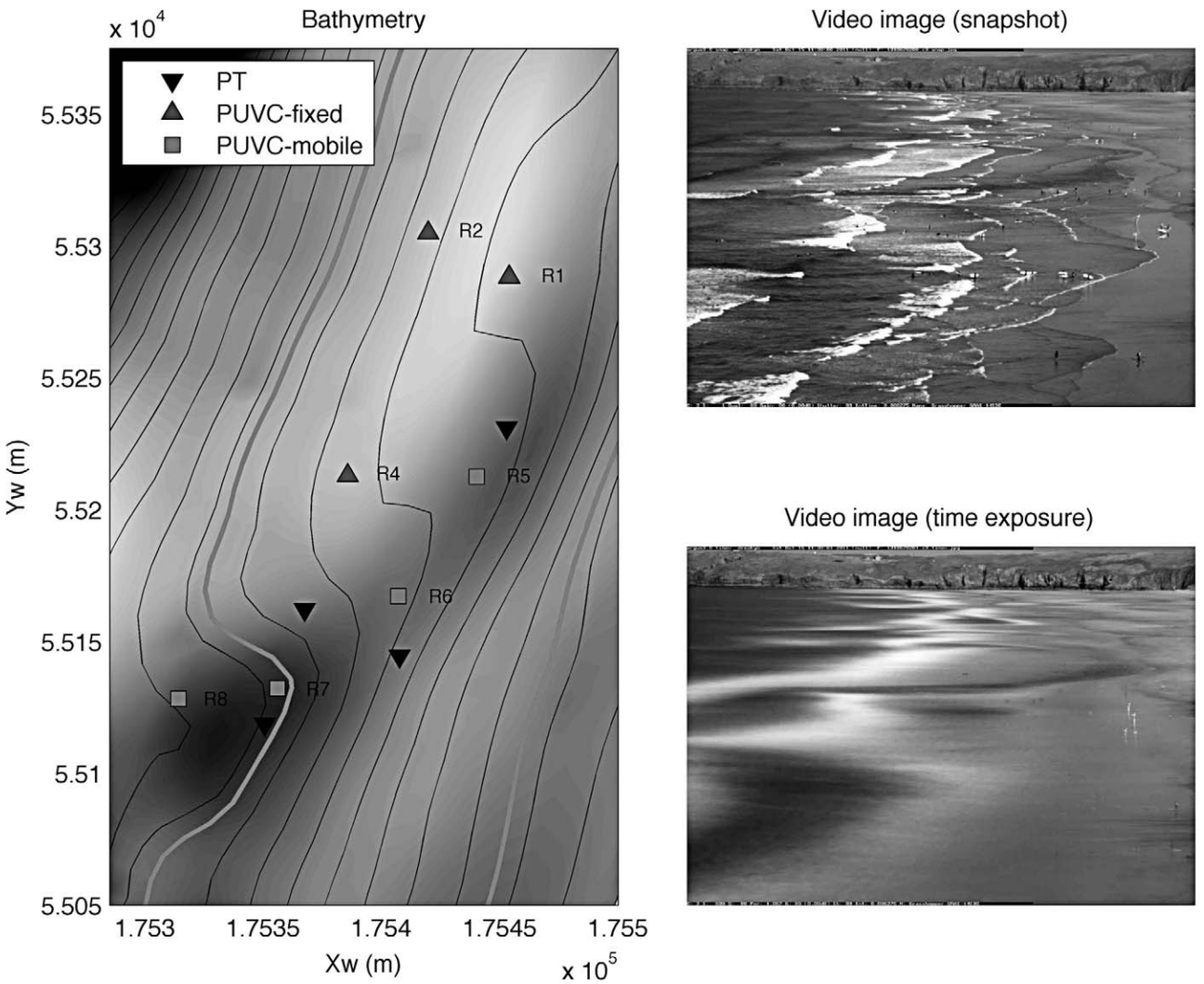

Figure 3. Examples of a typical rip current system during DRIBS rip current experiment. (Left panel) Local rip study region (0.25-m bathymetric contours and shaded residual morphology) showing typical Eulerian instrument deployment for experiment D2. Magenta contours indicate mean spring and mean neap low water levels. (Right panels, top to bottom) ARGUS video snapshot of the rip current system around low tide, and corresponding ARGUS video time exposure image (10-min) showing wave dissipation pattern over nearshore sand bar system (high-intensity bands).

alongshore-orientated array with two rigs along the feeder channel (R5 and R6), each mounting a three-dimensional acoustic Doppler velocimeter (3D-ADV), PT, and OBS, and two rigs (R7 and R8) in the rip channel, each mounting a pulse-coherent acoustic Doppler current profiler (PC-ADCP), PT, and OBS. All of the instruments were self-recording and sampled at 4 Hz, with the exception of the PC-ADCPs, which recorded vertical profiles at 1 Hz. During experiment D2, the same range of instruments, minus R3, but with the addition of 3D-ADVs to R7 and R8, were deployed in an alternative configuration designed to maximize spatial coverage over the bar/rip system (Figure 3). A total of 54 complete tidal cycles of data were collected during experiment D1 and 33 during experiment D2.

A typical example of the Eulerian data collected during the DRIBS field experiments is shown in Figure 4. Water depth at all instrument rig locations varied with the semidiurnal tide, but whereas R4 and R8 remained submerged for the duration of the tidal cycle, R5 in the feeder channel emerged at low water. Wave heights were also modulated at the tidal frequency, with the largest wave heights recorded over the bar crest during the flood tide. During this tide, H_s decreased by $\sim$0.3 m over the tidal cycle. The strongest flow velocities occurred when waves were breaking over the bar crest, typically when the water depth was less than 3 m. Over the bar crest, strong onshore and northerly-directed flows were recorded during the flood tide. In the feeder channel, cross-shore flows were quite small, but

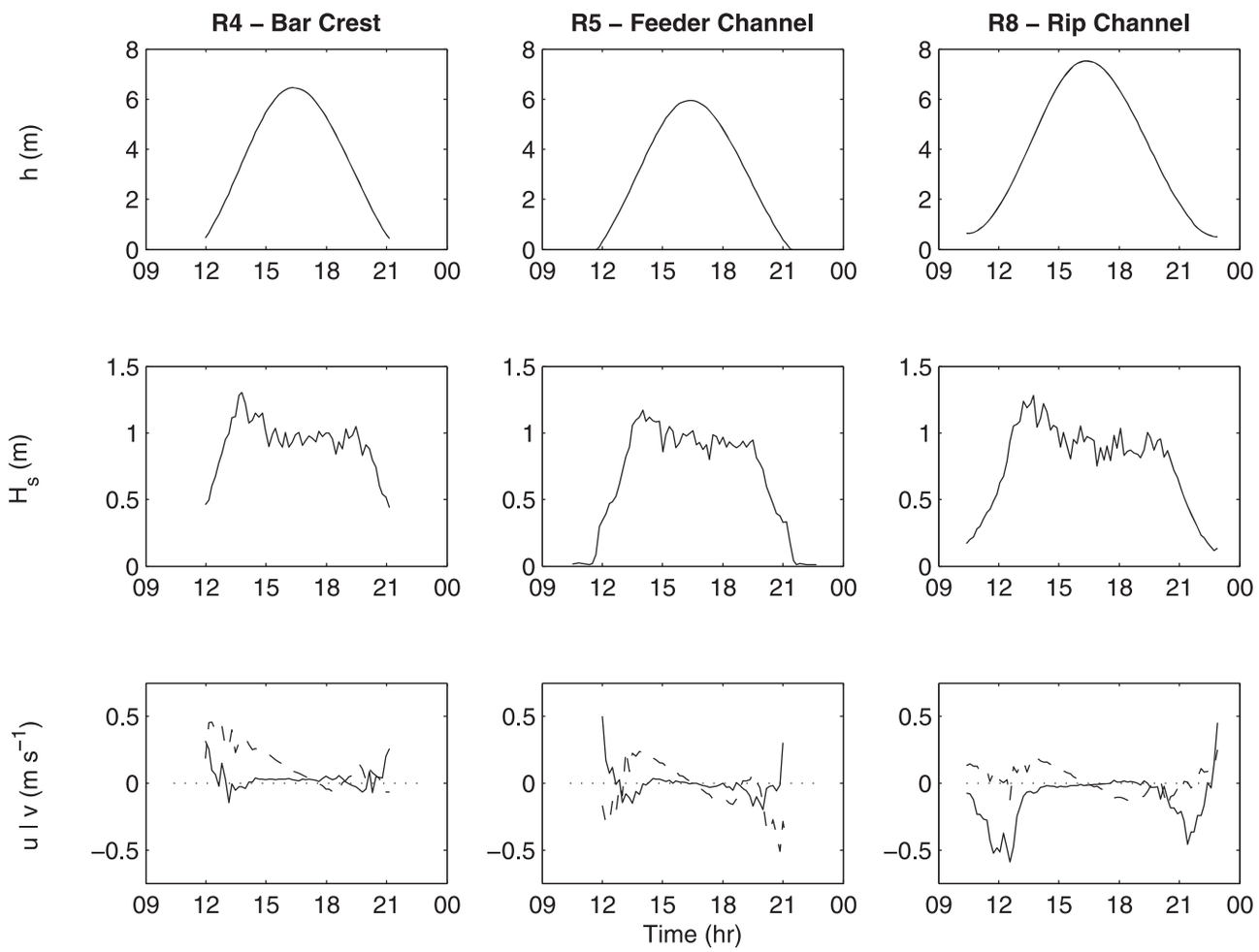

Figure 4. Example of 10-min time-averaged Eulerian data collected over Tide 30 on 26 October 2011 for three different locations in the bar-rip system. (Top to bottom) Water depth h; significant wave height H_s; and cross-shore u (solid line) and alongshore v (dashed line) flow velocity.

strong alongshore-directed flows toward the south prevailed during the shallow flood and ebb tide periods. In the rip channel, strong offshore-directed mean flows of 0.6 m s^{-1} occurred during the flood and ebb when water depth was less than 3 m; alongshore flows were generally weak. An interesting observation is the flow reversal in the alongshore currents either side of high water, suggesting a switch in the direction of the offshore tidal stream. This was a systematic observation throughout both field deployments, which does not appear to be linked to any specific wave conditions.

Lagrangian Data

Fifteen GPS-tracked surf zone drifters were used to record the Lagrangian currents over the bar/rip system. The drifters were of a robust design modified from that of Schmidt *et al*. (2003) and were modular in nature, allowing any damaged components to be easily replaced in the field. A detailed description of the drifter design and validation of using low-cost GPS technology for making valid and useful observations within a surf zone environment can be found in Schmidt *et al*. (2003), Spydell *et al*. (2007), and MacMahan, Brown, and Thornton, (2009). Our GPS units were custom-made in-house and recorded the raw L1 GPS carrier-phase information, which was logged to a secure digital high-capacity memory card at 1 Hz. The raw GPS data were postprocessed from a static Trimble base station to provide an accuracy of <0.4 m in horizontal position and <0.01 m s^{-1} in velocity. Following Murray (1975), the effects of wind slippage and drifter acceleration times were computed giving a maximum windage error of 0.1 m s^{-1} and demonstrating that the drifter speeds were within 10% of the mean current within 6–12 s of deployment.

Drifter deployments were for 3–5-hour periods centered on low tide when the rip currents were most active. Drifters were individually seeded (rather than in clusters) from the beach

into the feeder and rip regions to maintain both spatial and temporal coverage across the bar/rip, maximizing the synoptic understanding of circulation patterns through the rip system. Due to the rate of change of tidal elevation within a macrotidal regime, it is desirable to have drifter observations throughout the entire rip system at least every 30 minutes. Drifters were removed from the water using an RNLI inshore rescue boat when they either exited the surf zone seaward or traveled alongshore out of the measurement region. If washed ashore, the drifters were removed by manual operators. The typical extent of the drifter deployment region was ~500 m in the alongshore and ~300 m in the cross-shore (Figure 3). In total, drifters were deployed for 25 days, providing ~100 hours of Lagrangian data.

Once the drifter data were postprocessed to provide positional information, the behavioral characteristics of the individual drifter tracks (with points recorded at 1 Hz) were analyzed, and the mean drifter circulation patterns were calculated (Figure 5). The example data shown in Figure 5, representing 163 separate and independent drifter deployments, are predominantly a mixture of rip exit and rotational circulation behaviors. Individual drifters deployed around the MLWS elevation typically move alongshore before a proportion turn ~90 degrees and travel seaward in the rip channel. Subsequently, drifters exit the surf zone, travel alongshore or rotationally circulate back toward the shoreline over the intertidal bar. Drifters that do not enter the rip feeder/channel either wash up at the shoreline, travel alongshore, or display no characteristic behavior. During this sample deployment, and with reference to the bottom-right panels of Figure 5, 47% of drifters entered the rip current (Rip); of these, 23% exited the surf zone seaward by moving offshore of the breaker line (EX), 1% moved alongshore (AL), and the remaining 23% rotated back toward shore (RO). At least 40% of the rotational-mode drifters completed a full rotation, and one of the GPS drifters completed nine cycles over the measurement period.

A 10 × 10-m regular grid was defined across the surf zone, and the mean drifter pattern was computed. First, the number of individual drifter passes per grid cell was calculated, and cells containing fewer than three individual passes were discarded. Second, the number of independent observations per bin was calculated following Spydell *et al.* (2007). If a drifter enters the bin only once, it is counted as an independent observation. If the drifter leaves the bin, remains outside of the bin for longer than it would take a drifter to cross the bin (determined by an average of all measurements in the bin), and then re-enters the bin, it is counted as a new drifter entering the bin and therefore an independent pass. Velocities within bins containing at least three independent passes were averaged to provide the mean circulation pattern.

The mean drifter circulation pattern in Figure 5 clearly demonstrates the propensity for drifters to exit the surf zone during this tide, with an expanding rip head region seaward of the outer surf zone edge. A small rotational eddy is clearly present in the center of the rip domain, with an approximate 50% split in drifters entering the rip channel rotating back toward the shoreline or exiting seaward. The strongest rip speeds are located in the rip channel, before the flow diverges into rotation or exit, and flows can exceed 1.6 m s^{-1}. Flow speeds in the feeder channel are weaker, typically around 0.5–0.8 m s^{-1}.

ARGUS Remote Sensing

A permanent ARGUS video system (Holman and Stanley, 2007) is deployed at Perranporth on the cliffs at the southern end of the beach. It utilizes two cameras to provide an overview of the entire beach and a third (zoomed) camera specifically focused on the bar/rip regions. The system collects the standard suite of ARGUS image products every 30 minutes, and images from all three cameras were merged and rectified to provide plan-view timex images (Figures 1 and 3). A meteorological station equipped with an ultrasonic anemometer recording wind speed and direction every 30 minutes is deployed with the ARGUS station.

Behavioral Summary

The DRIBS fieldwork of 2011 (and the earlier work of Austin *et al.*, 2011) has indicated that the kinematics of the Perranporth rip systems are complicated, with different circulation patterns and flow speeds controlled by the combination of tide and waves, further influenced by the wind.

The rip currents are constrained by the intertidal morphology and are only active when the sand bars are exposed to waves. Therefore, because of the dominant LTBR morphology, the rip channels are located around the spring low-tide shoreline, and the rip currents are only active for 2–3 hours centered on low tide (Figure 4). The strongest rip current velocities are typically measured during moderate to energetic wave conditions. However, as the surf zone tends toward saturation and displays greater alongshore-uniform wave breaking during more energetic conditions, the rip currents become less distinct, and the dominant flow direction becomes increasingly alongshore. Observations suggest that wave breaking across the subtidal bar during the more energetic conditions essentially closes off the rip channel, thereby minimizing the number of surf zone exits. Strong alongshore winds further enhance this transition toward alongshore-dominated, rather than offshore-directed, flow (Earlie, 2011).

DEVELOPMENT OF RIP RISK PREDICTION TOOL (RRPT)

RRPT Model Architecture

The RRPT model can be subdivided into three core sections: (1) a regional wave model, (2) a local, two-dimensional horizontal (2D-H) wave and flow model, and (3) risk allocation and dissemination. Each section operates as a standalone process, with the results being linearly passed along the process chain (Figure 6). The physics of the numerical models will not be discussed here because comprehensive analyses of their performance already exist in the literature, but validation of the models' performance is demonstrated for this application.

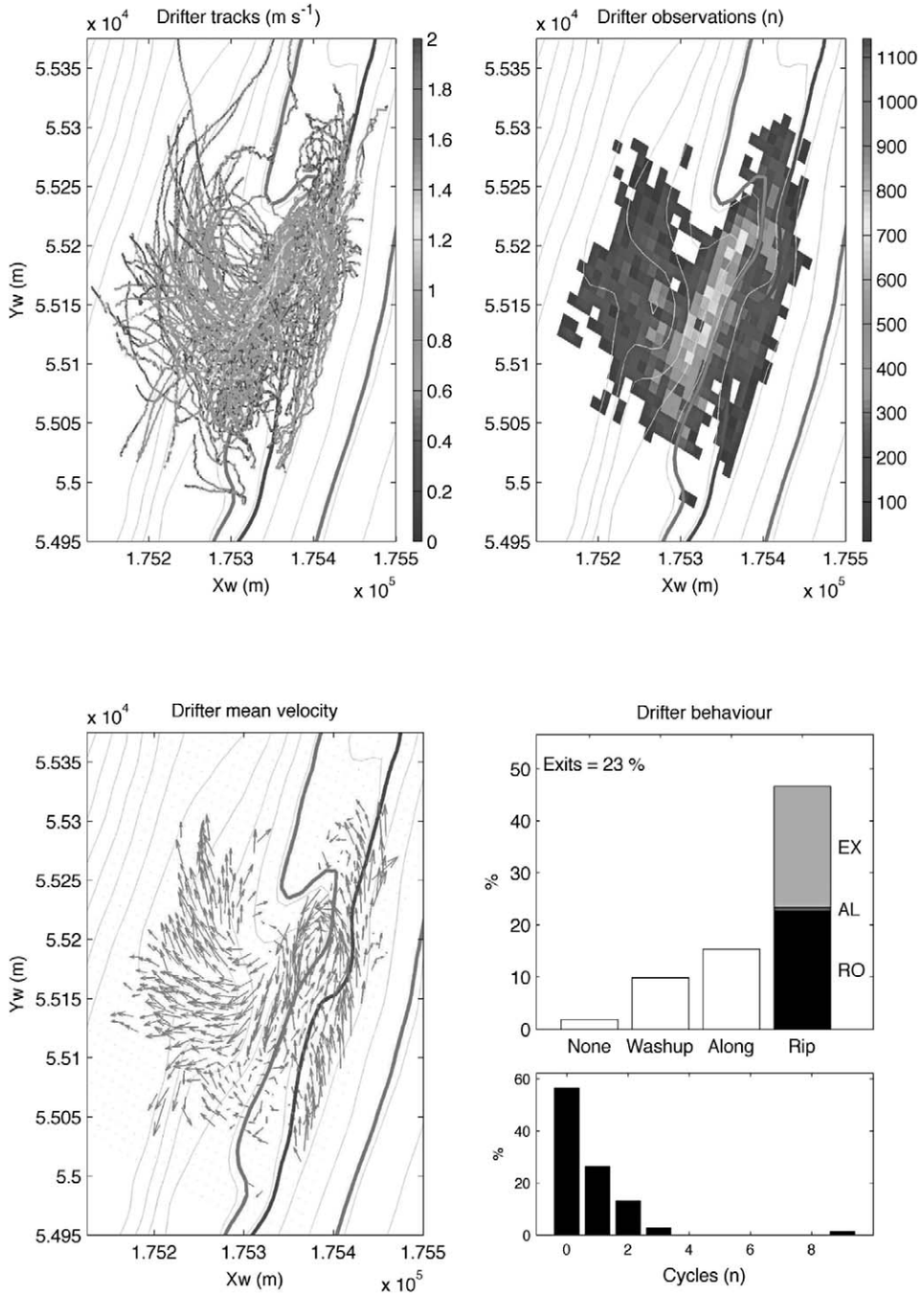

Figure 5. Example of Lagrangian drifter data and processing pathway. (Top left) Individual tracks from each individual drifter deployment colored by drifter speed. (Top right) Number of significant individual drifter observations. (Bottom left) Mean drifter circulation pattern with contours of elevation. Arrow length is proportional to rip speed. The MLWS elevation (blue) and the maximum and minimum tidal elevations during the deployment (magenta) are highlighted. (Bottom right) Behavioral classification for each drifter track, where EX represents drifters exiting the surf zone, AL is alongshore movement, and RO is drifters that rotated back to shore. (Color for this figure is only available in the online version of this paper.)

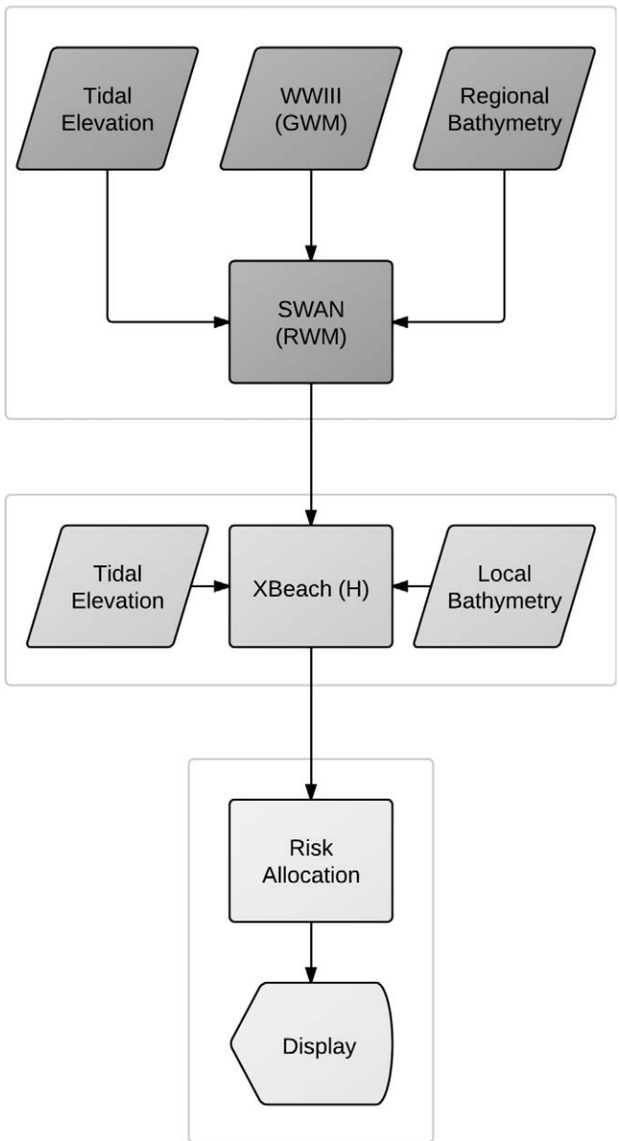

Figure 6. Flow diagram of RRPT model architecture. Regional wave forcing (dark gray), local hydrodynamic flow and wave model (medium gray), and risk allocation and dissemination (light gray).

Regional Wave Model (RWM)

The input wave forcing to the RRPT is provided by an operational version of the simulating waves nearshore (SWAN) wave model (Booij, Ris, and Holthuijsen, 1999) run on a regional scale around the southwest peninsula of the U.K. (Coastal Processes Research Group, 2012). The SWAN RWM runs in nonstationary mode over a 200 × 160-km regular spherical grid with a 5-km node size. It is run daily with initial wave and wind forcing provided by the U.S. National Oceanic and Atmospheric Administration WWIII (Tolman, 1997) Global Wave Model output (t00z run time) applied along the complete northern, western, and southern boundaries, providing a forecast for a 27-hour period. Integrated wave parameters are output at 30-minute intervals across the entire domain and at a range of points around the coastline that correspond to the locations of permanently deployed inshore wave buoys. At the Perranporth location, a 12 × 15-km grid with 150-m node size is nested within the RWM and outputs 2D spectral data (*.sp2* files), also at 30-minute intervals, at a location coincident with the Channel Coastal Observatory (CCO) inshore wave buoy (Figure 7).

The model output has been compared with the CCO wave buoy over a 2-month period. The buoy data for 0300 GMT on d_n (where d = day) is compared with the SWAN forecast for d_n and d_{n-1} (t00z run time), thus comparing model skill for forecasts of 3 and 27 hours (Figure 7). The overall model skill is good, with both the mean trends and finer detail in all of the integrated parameters well predicted. The key areas in which the model skill is degraded is at the onset of new long-period swell events, where the peak H_s is underestimated and the increase in wave period is lagged by several hours. This is probably because of the input forcing of the WWIII model, whereby any timing offset of the longest period swells entering the WWIII domain will propagate unmodified with those waves across the domain. A drop-off in model skill for the 27-hour forecast occurs with greater scatter in the data.

The model skill has been quantified for H_s, T_p, T_m, and D_p computed with the use of a range of standard indices (refer to the Appendix for a description of the indices) for the 3- and 27-hour forecasts (Table 1). The slope and intercept values for the best-fit correlations are also reported. It should be noted that the R^2 values for D_p are low because of the limited spread of the data due to the directional resolution of the model.

2D-H Wave and Flow Model (XBeach)

The XBeach model (*cf.* Roelvink *et al.*, 2009) is used to solve coupled 2D horizontal equations for wave propagation and flow for varying spectral wave and flow boundary conditions. XBeach includes a nonstationary wave driver with directional spreading, which accounts for wave group–generated surf motions that are important for rip current dynamics (*e.g.*, MacMahan *et al.*, 2004). For this application, XBeach is run only in hydrodynamic mode without sedimentation or morphological updating to minimize computational time.

The bed level for the XBeach model is based on the combined bathymetric and topographic survey data measured at the time nearest the simulation time of interest. The computational grid is generated, optimizing the spatial resolution across the surf zone in the center of the model domain, which is 860 × 1220 m in the cross- and alongshore directions, respectively. The wave conditions at the offshore boundary of the XBeach model are described by the 2D spectral output from the nested SWAN model appropriate to the simulation time. The tidal level is varied from start to end of the simulation on the basis of a local prediction derived from the harmonic analysis of a long-term dataset.

The XBeach model has a number of free parameters that are used to calibrate the model. In our hydrodynamic-only model,

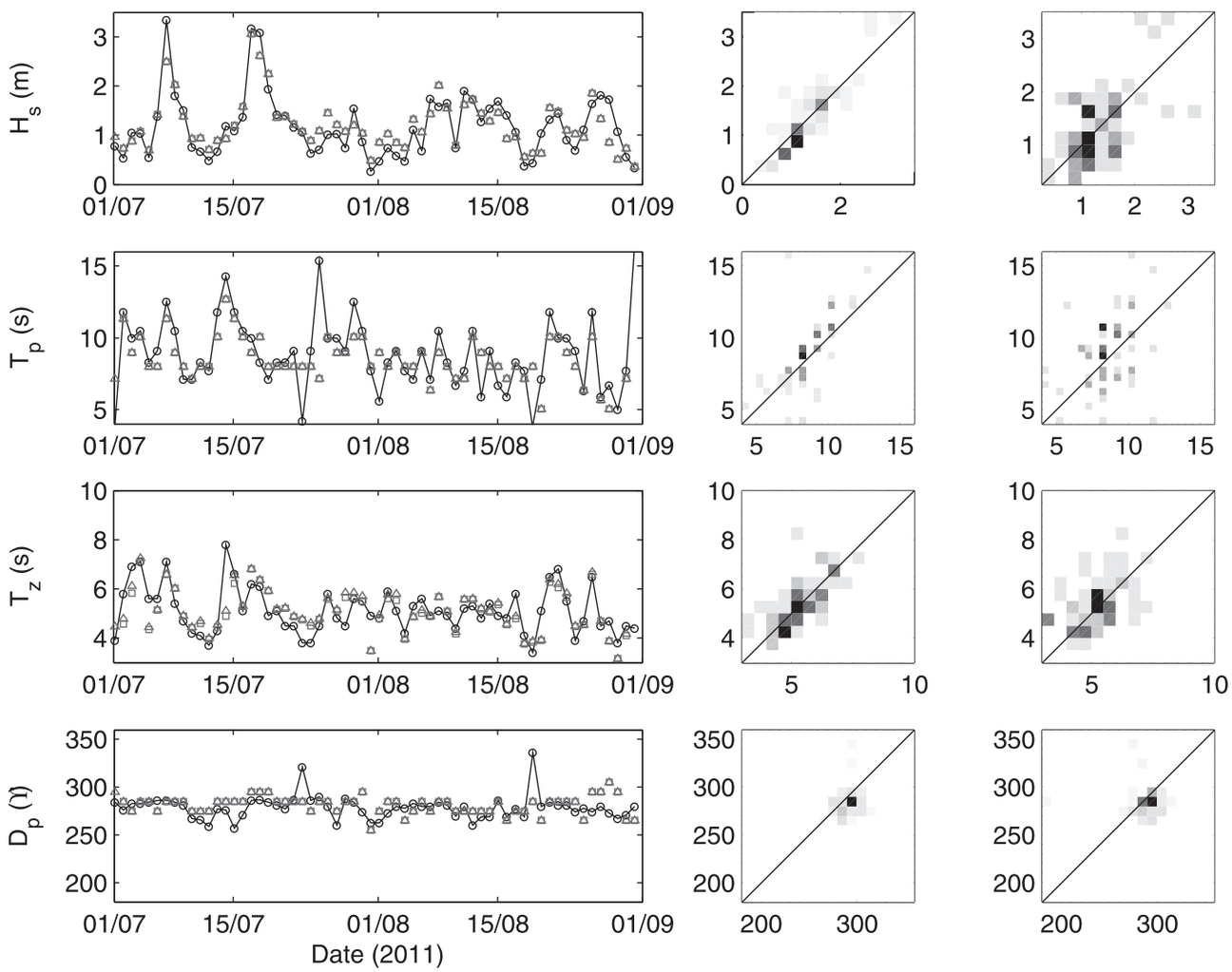

Figure 7. (Left panels) Time series of integrated wave statistics measured at the CCO wave buoy (black) with those computed by the SWAN RWM forecast at t00z + 3 h (blue) and t00z-1 + 27 h (red). (Center and right panels) Joint distribution of buoy (horizontal axis) and SWAN RWN (vertical axis) wave statistics for t00z + 3 h forecast (center) and t00z + 27 h forecast (right). Color scaling is incident of occurrence, with darker colors representing greatest occurrence. Black line plots the 1 : 1 slope.

the parameters that required tuning were those governing the short-wave breaking, the breaker formulation (break), and the breaker slope coefficient in the roller model (β). All other parameters were set to their recommended default values. The hydrodynamics of the model are calibrated with measured Eulerian data, and the nearshore circulation patterns were validated against Lagrangian drifter measurements.

To verify the 2D-H hydrodynamics of the XBeach model, a simulation was set up, forced by a directionally spread spectral input, to compare measured and computed hydrodynamics. The period that is modeled is 13 June 2011, which represents Tide 54 during the first DRIBS field deployment, where H_s at the seaward boundary of the model was 1.05 m, with $T_p = 9.1$ s and a mean angle of incidence of –5° relative to the shoreline. The model was run for a 30-

Table 1. *SWAN RWM skill indices. Correlation coefficient (R^2), scatter index (SCI), relative bias (Rel. bias), and slope (a) and intercept (b) of linear regression.*

Parameter	R^2	SCI	Rel. bias	a	b
3-h forecast					
H_s	0.88	0.22	0.02	0.72	0.35
T_p	0.43	0.26	−0.05	0.3	5.72
T_m	0.71	0.13	0	0.7	1.52
D_p	0.26	0.05	0.01	0.2	225.42
27-h forecast					
H_s	0.55	0.41	0.01	0.47	0.64
T_p	0.13	0.33	−0.06	0.1	7.36
T_m	0.44	0.19	−0.03	0.47	2.57
D_p	0.02	0.14	−0.01	−0.07	296.91

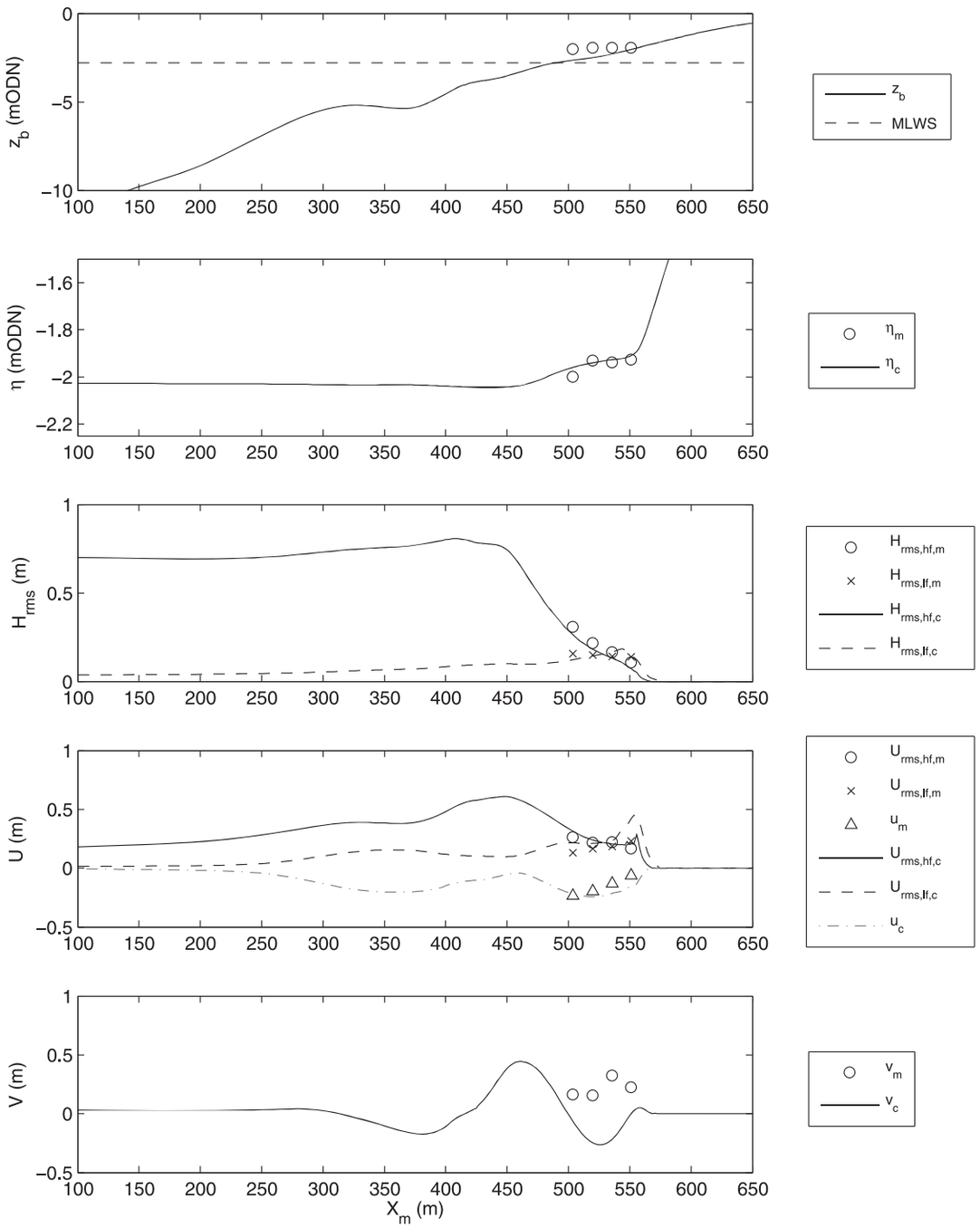

Figure 8. XBeach Tide 54 comparison of measured (subscript m) and computed (subscript c) hydrodynamic parameters. (Top to bottom) Beach profile z_{oo} indicating instrument rig locations and MLWS; measured η_m and computed η_c water surface elevation; measured and computed RMS wave height of the short $H_{rms,hf}$ and long $H_{rms,lf}$ waves; cross-shore RMS velocity of the short $U_{rms,hf}$ and long $U_{rms,lf}$ waves and mean cross-shore velocity u; and mean alongshore velocity v. In the panels comparing field data with model predictions, markers are used for the observations and lines for the predictions.

minute period, during which time the water depth over the intertidal bar was ~1 m. This period was chosen because all of the instruments were functioning and fully submerged, the waves were sufficient to generate a significant infragravity component in the spectrum, and the water level was such that rip-type circulation was active within the surf zone. The model was set to provide output over the cross-shore transect of instrument rigs R1–R4 to compare the

Table 2. *Summary of error statistics (refer to the Appendix for a detailed description of the statistics).*

Parameter	R^2	SCI	Rel. bias
η	0.65	0.01	0
$H_{\mathrm{rms,lf}}$	0.72	0.13	0.01
$H_{\mathrm{rms,hf}}$	0.83	0.17	−0.17
$U_{\mathrm{rms,lf}}$	0.74	0.51	0.39
$U_{\mathrm{rms,hf}}$	0.67	0.15	0.09
$\langle u \rangle$	0.03	0.43	0.19
$\langle v \rangle$	0.15	1.71	−1.60

evolution of the wave and flow field during wave transformation and dissipation across the surf zone and, in particular, the intertidal bar (Figure 8).

Modeled time-averaged water levels are compared with the time-averaged measurements at R1–R4 in the second panel of Figure 8, and the observed wave set-up across the surf zone is well predicted. In the third panel of Figure 8, it can be seen that the XBeach model very closely predicts the magnitude and cross-shore trends of both the infragravity and short-wave heights. The short-wave cross-shore flow velocity measurements and predictions also compare well, but there is an overestimation of the infragravity velocities close to the shoreline. The magnitude and distribution of the mean cross-shore flow velocity is well predicted. The measured and modeled time-averaged alongshore current is shown in the final panel of Figure 8. The model predicts the incorrect direction for the alongshore-directed current, and this is probably related to its directional instability around the rip morphology, where rotational circulation in particular can cause a current reversal in the space of one or two grid cells. The results were somewhat sensitive to the choice of values for *break* and β. These were changed from their default values and set to *break* = 4 the advective-deterministic approach of Daly *et al*. (2012), which allows wave breaking to start and stop over complex bathymetry, and $\beta = 0.05$, which reduces the slope of the face of the wave roller. The correlation coefficient, scatter index, and relative bias for the simulation are shown in Table 2, and these compare favorably with the values of Roelvink *et al*. (2009) for the Delilah field test case.

The nearshore circulation patterns predicted by the XBeach model were validated against measured Lagrangian data. The three most characteristic modes of circulation observed during the field experiments using the GPS drifters were alongshore, rotation, and exit. Three drifter deployments were selected from the data set, each displaying one of these dominant circulation modes, and the XBeach model was run for the corresponding time period, with varying tidal elevation and the input wave forcing predicted by the SWAN model. The model was seeded with virtual drifters at the same times and locations as the GPS drifters, and the results were compared with the measured data. The virtual drifters propagate at the Generalized Lagrangian Mean (GLM) velocity and thus include the effect of Stokes drift. The location of the seaward edge of the surf zone was used to define a drifter exit and was computed as the cross-shore location where the alongshore-averaged roller dissipation exceeds 10% of the cross-shore maximum ($DR_{10\%}$). For the model simulations, roller dissipation is a standard output, whereas for the measured field data, it was computed using the ARGUS video data following van Dongeren *et al*. (2008).

Application of the XBeach model yields flow patterns that are remarkably similar to the field observations for each of the 3 days (Figure 9). The alongshore mode occurred during energetic conditions with a wide surf zone, and flows are toward the south and constrained in the trough between the low-tide shoreline and inner bar crest. The simulated drifters move slightly farther seaward, following the depth contour around the southern extent of the rip current, but do not move into the seaward trough.

The rotational mode shows onshore flows over the shallow bar crest feeding southward into the rip channel and flowing seaward in a clockwise rotation. The virtual drifters produce a similar rotation, which is slightly compressed in the cross-shore, and also displays the counter rotation to the south of the rip channel. Again, the drifters do not exit the surf zone.

During the exit mode, drifters flow south along the feeder channel between the crest of the inner bar and the shoreline before flowing seaward through the rip channel and exiting the surf zone by moving offshore of the $DR_{10\%}$ limit. The modeled rip current is, however, significantly narrower than the observed rip current. Small clockwise rotational modes are also evident at the southern terminal of the inner bar, and a counter-rotation is present to the south of the rip channel.

The mean computed Eulerian flow patterns, together with the GLM velocity field, for the three simulations are shown in Figure 10. Toward the offshore edge of the surf zone and for offshore-directed flows, the Eulerian and GLM velocities are almost identical. However, moving landward to the inner surf zone, the GLM flows are deflected farther landward, increasing surf zone retention and, where rotational circulation is present, display a smaller radius (tighter circulation). This result is very similar to that of Reniers *et al*. (2009), who also used a wave group–resolving modeling approach to simulate surf zone circulation on a rip-channeled beach, and reinforces the importance of including Stokes drift in calculating surf zone circulation.

The individual drifter tracks, which when averaged form the distinct circulation patterns observed in Figure 9, were analyzed to fully qualify their behavior. Drifters were broadly classified into two initial classes: (1) those that entered the rip circulation during their deployment (*i.e*., entered the rip neck or feeder regions) and (2) those that did not. Group 1 were then further classified as exits (moving seaward of the surf zone), rotation, or alongshore. Similar classifications were applied to group 2: alongshore, shoreline wash-up, or none (no distinct behavior).

A comparison of the behavior of the measured and modeled drifters, as classified above, is provided in Figure 11. It is very encouraging to observe that for the drifters that entered the rip circulation, the measured and modeled proportions of behaviors are very similar, the only significant difference being the increased percentage of modeled exits for 29 May (rotation). As discussed by Reniers *et al*. (2009), it is possible that the inclusion of very low frequency motions with $O(10)$-minute timescales increased surf zone retention and reduced the number of exits. For the group of drifters that did not enter the rip circulation, the behavior is less well reproduced for 29 May

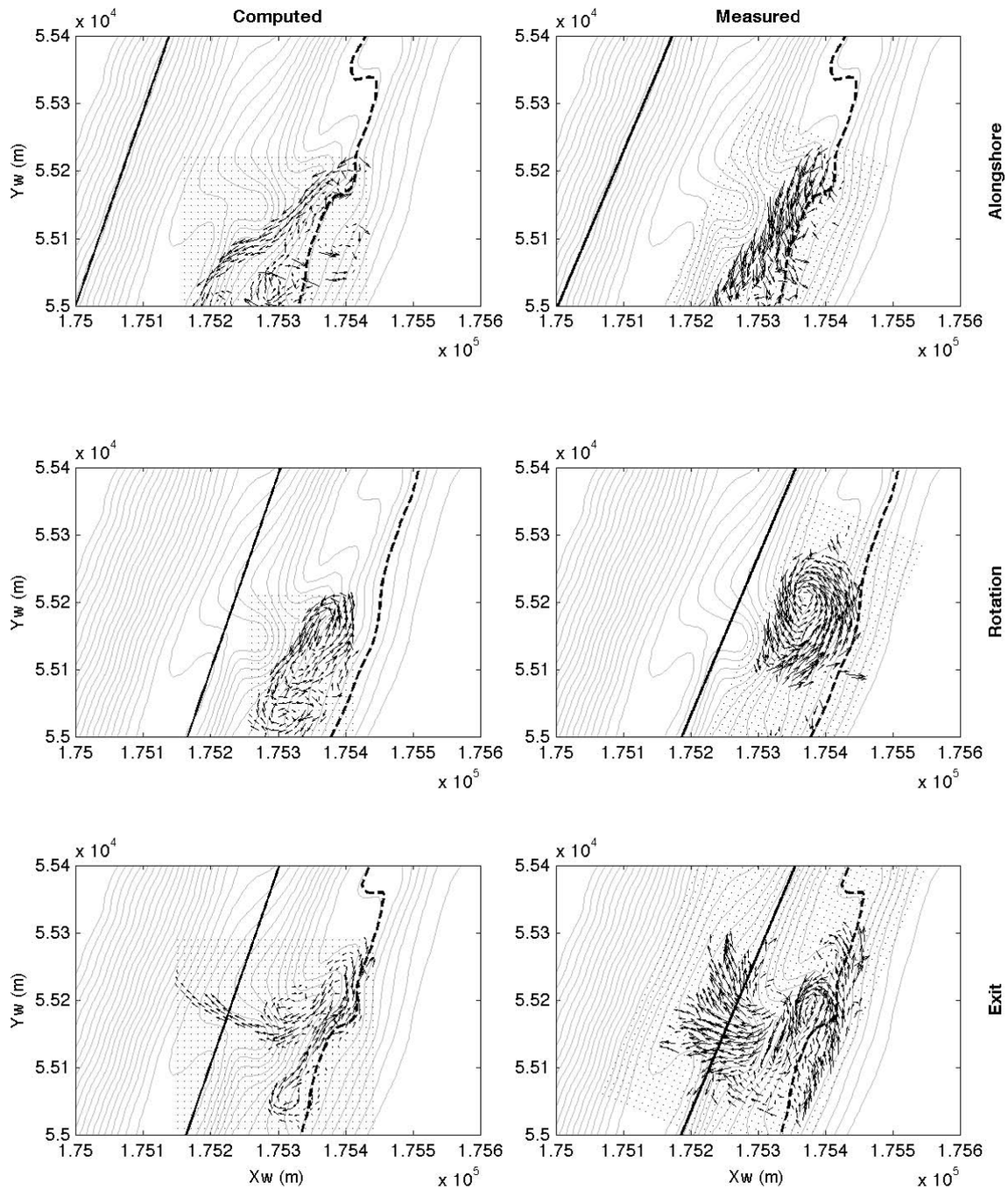

Figure 9. Mean circulation patterns for drifters averaged over the deployment windows from the field measurements. (Left panels) XBeach-computed drifters. (Right panels) Measured drifters. Bathymetry is contoured in the background at 0.25-m intervals; the dashed contour indicates the low-tide water level, and the solid black line is the corresponding seaward edge of the surf zone. The quivers indicate drifter direction.

and 16 June, with an underprediction of alongshore and wash-ups, respectively. Rip circulation is highly complex and three-dimensional, and Figures 9, 10, and 11 indicate that the dominant mode of circulation is well predicted by the model for all three of these test cases—alongshore, rotation and exit—although some of the finer detail is not reproduced. Overall, the comparison between model predictions and field observations is considered very favorable.

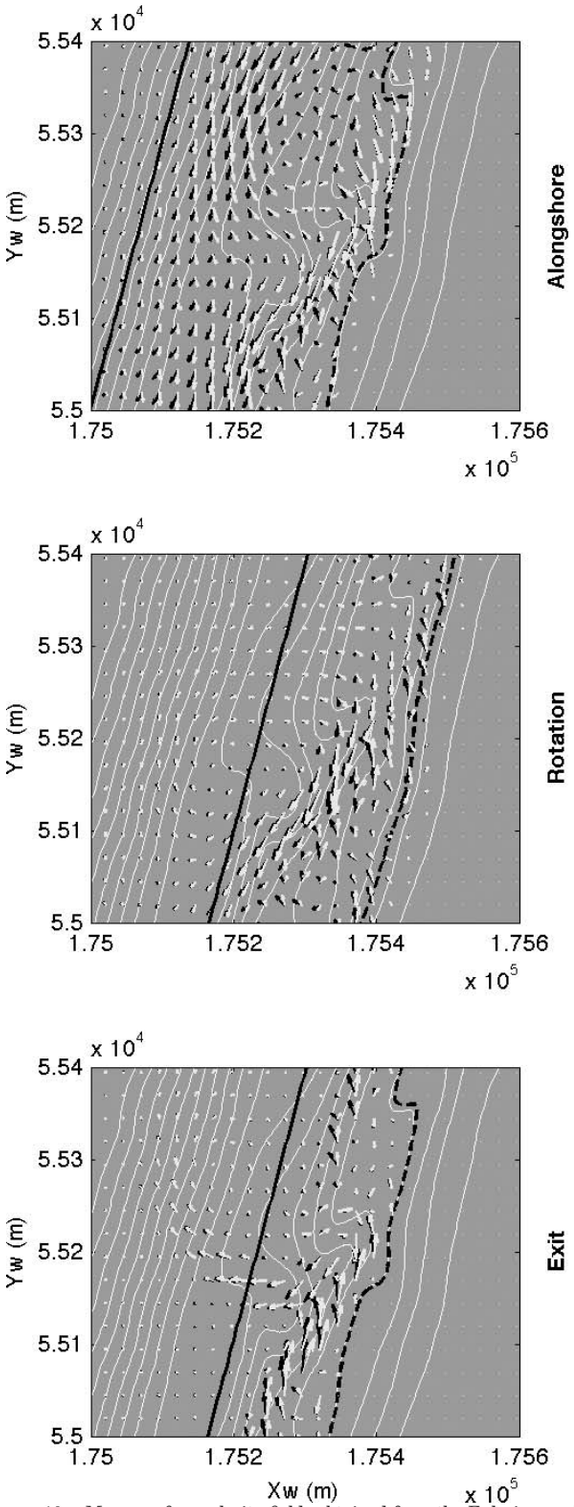

Figure 10. Mean surface velocity fields obtained form the Eulerian model predictions (black arrows) and GLM computations (yellow arrows). Bathymetry is contoured in the background at 0.5-m intervals; the dashed contour indicates the low-tide water level, and the solid black line is the corresponding seaward edge of the surf zone.

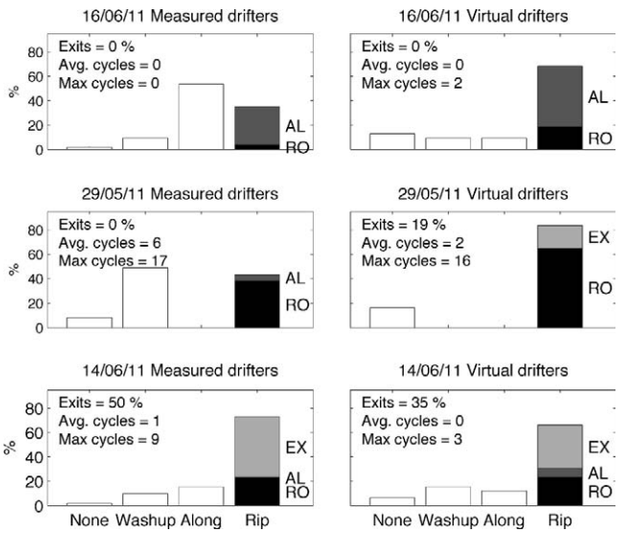

Figure 11. Comparison between measured and modeled behavioral classification of Lagrangian drifter motions. Legend entries: EX = exits; AL = alongshore; and RO = rotation within the surf zone.

MODEL APPLICATION

Tidal Cycle Simulation

A model simulation was run over a tidal half-cycle for 15 August 2011, and the surf zone circulation patterns were visualized at 30-minute intervals to demonstrate flow variability for different stages of the tide (Figure 12). The simulation was initialized at midtide ($\eta = 0$ mODN) 3 hours before low water, when mean flow velocities in the surf zone are weak ($\sim$0.1 m s^{-1}) with no defined flow through the rip channel. As the tidal elevations fall, offshore-directed flow is rapidly established in the rip channel with onshore flow over the bar crest at $Y_{xb} = 1300$–1500 m and a small rotational cell to the south at $[X_{xb}, Y_{xb}] = 750, 1100$ m feeding the rip current. By low water (LW) – 1 hr, mean rip current speeds are 0.8 m s^{-1}. It is noteworthy that the landward end of the rip current is located in very shallow water close to the shoreline over the low tide period, maximizing the exposure of bathers to the hazard. As the tide subsequently floods, rip speeds decrease and the rip current effectively moves seaward, with only a weak offshore flow >150 m from the shoreline.

Daily Hazard Forecast

The RRPT model suite was run in forecast mode to provide an example prediction of rip current flows over a 24-hour period. The model was initialized with SWAN RWM 27-forecast output for 02 September 2011, and the XBeach component ran a 15-minute simulation every hour for the 24-hour period beginning 0300 hours on 02 September 2011. The 15-minute–averaged values of rip flow speed (U_{rip}), flow direction, tidal level, and root mean square (RMS) wave height were output from 30 × 50-m regions containing 16 grid nodes over the rip channel and bar

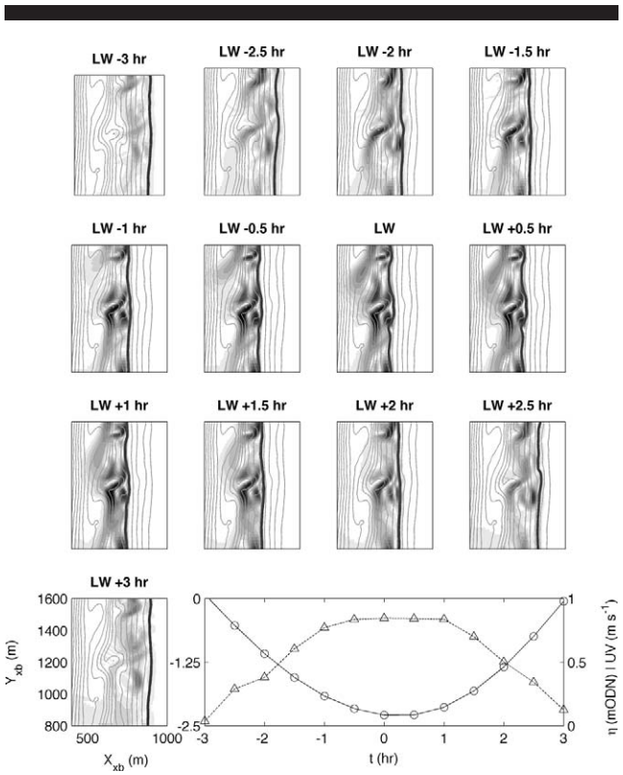

Figure 12. Flow patterns for different stages of a tidal cycle on 15 August 2011. Contour plot bathymetry; background shading is 30-min mean velocity magnitude with white = 0 m s^{-1} and black = 1 m s^{-1}; heavy contour is the shoreline. Bottom right panel plots tidal elevation (left axis, circles) and flow speed (right axis, triangles) in the rip channel. Axes are shown plotted on the XBeach computational grid (X_{xb}, Y_{xb}).

crest (Figure 13). U_{rip} can be problematic to define (*e.g.*, Castelle *et al.*, 2010), and for this case, we define U_{rip} as the maximum velocity magnitude, with an offshore-directed flow component,

$$U_{rip} = \sqrt{\overline{u_{off}^2} + \overline{v^2}} \quad (1)$$

where u_{off} is the offshore-directed flow velocity, v is the alongshore-directed velocity, and the overbar signifies time averaging.

Maximum rip speeds were predicted for the period 2 hours either side of low water during the 24-hour forecast. This suggests that the rip hazard is maximized at 0000 hours, 0900–1300 and 2100–2400 hours, when the water depth in the rip channel is <2.5 m. Local wave height increases from 0.9 to 1.2 m during the forecast period.

MODEL EVALUATION

Hindcast model predictions of rip current occurrence and strength were compared with RNLI incidence records for July and August 2011. The model was run daily for a 4-hour period centered on the daytime low water, resulting in 62 tides of simulated data. The model was forced with SWAN RWM output, predicted tidal elevation, and the nearest available measured bathymetry (one in July, one in August). The 30-minute means of flow velocity were output every 30 minutes and subsequently averaged to provide daily mean estimates of the maximum offshore flow velocity and maximum rip speed.

The RNLI incident statistics consist of an hourly estimate of the number of people in the water and the number of rip current incidents occurring; incidents divided by number of people in the water provides a probability of incidence occurrence (individual incident risk) and a more appropriate indication of rip hazard levels (Figure 14). Incidents occurring outside of the low-tide tidal half-cycle were excluded from the analysis because they are related to fixed high-tide topographic headland rip currents, which are not the subject of this investigation.

Risk Allocation

One of the key aspects in the development of the RRPT is the process of allocating hazard levels to the model. In a standard risk model, risk is defined as the likelihood of exposure to a hazard multiplied by the severity of hazard. The hazard in this case is clearly defined as a rip current that can lead to drowning, but the key characteristics and controls on the severity of this hazard must first be defined.

If we assume that the principle hazards of a rip current are the flow speed and the proportion of rip exits, we can allocate ratings to each factor that will increase the hazard severity (likelihood of causing harm) for each. We must also apply a rating for severity of hazard to the flow speed and exits. High flow speeds have the potential to transport bathers out of their depth and into regions of high breaking waves, whereas high proportions of rip exits will move bathers offshore into deep water. The next stage is to combine the individual hazard ratings to compute an overall severity of the rip current hazard; in this example, assuming that the rip exit and flow speed factors carry equal weighting.

In this case, if the wave height is large, rip flow speeds may be very strong (high flow hazard), so the overall hazard level is high. However, large waves probably mean a wide saturated surf zone and low occurrence of rip exits (low exit hazard), so the overall hazard level is probably medium because flow speed and exits carry equal weighting in this case. Clearly, it is critical that the thresholds applied correctly categorize the perceived hazards so that periods of high risk can be identified by the end user, but also so that periods of low risk are not incorrectly flagged as hazardous, resulting in false alerts. Long-term records of lifeguard incidents (implicated with rip current activity) and beach user numbers provide a useful dataset to evaluate the skill of a chosen categorization for a given site. Indeed, in most cases, lifeguard records represent the only available data to define and test hazard categorizations.

Simple hazard ratings were applied to the XBeach model output by applying thresholds to the rip speed and drifter exits, which maximized the successful prediction of rip incidents while minimizing the number of false alerts (Table 3). The two scores were subsequently added together and rounded to integer values to provide a risk rating of 1–3, equating to

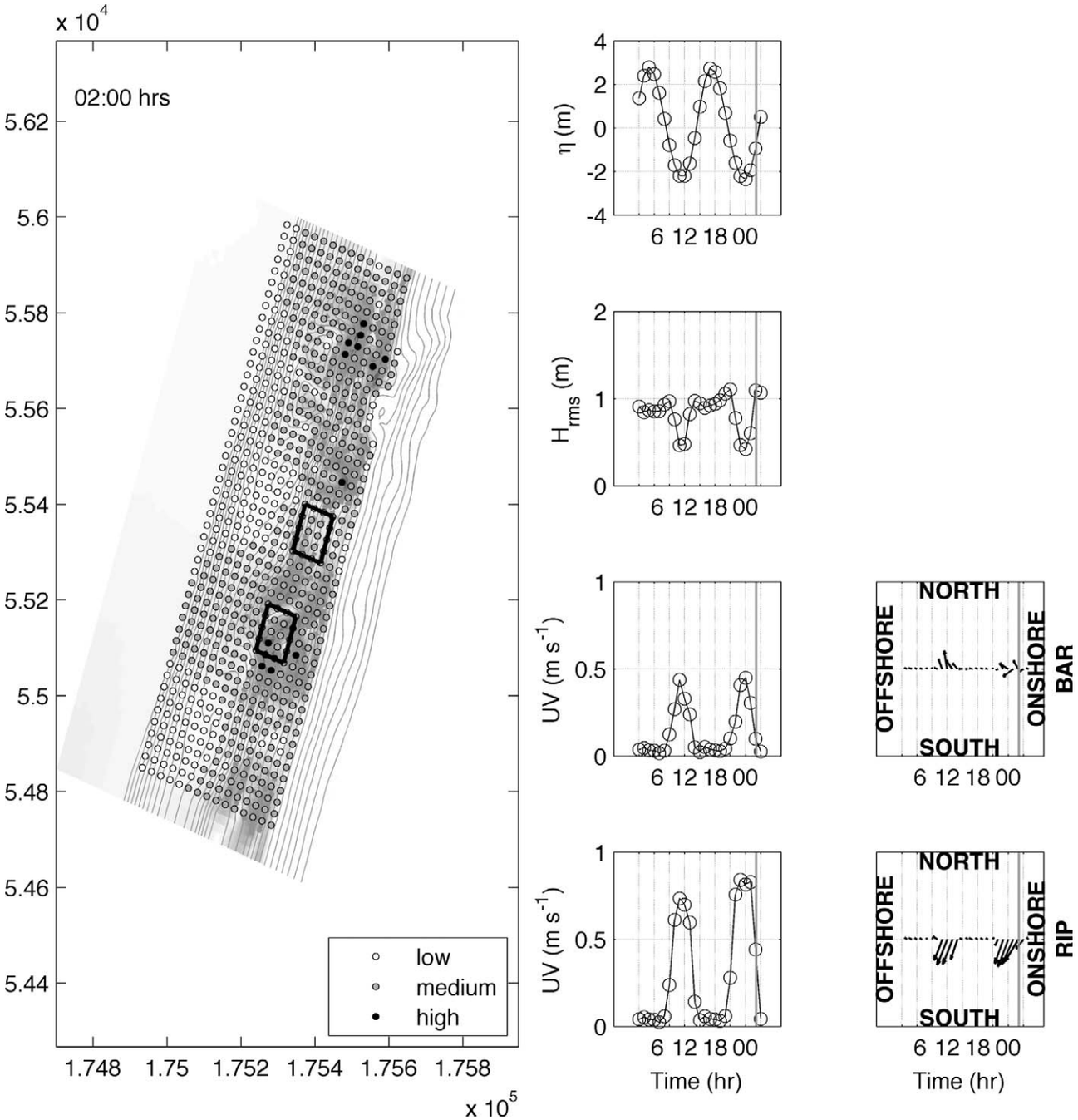

Figure 13. Model forecast for 24-h period. (Left panel) Mean current strength for a 15-min simulation with flow speed classifications; (right panels from top) 15-min mean tidal level, η; RMS wave height, H_{rms}; current speed, *UV*, and direction over the bar; and current speed, *UV*, and direction in the rip channel. Vertical patch represents the time interval of the surface plot.

low–high risk of rip current incidents occurring (Figure 14). Comparing the occurrence of total recorded rip current incidents and predicted hazard ratings, 64% of measured incidents occurred during predicted high-hazard conditions, 36% during medium-hazard conditions, and 0% during low-hazard conditions. Overall, the agreement between recorded individual incident risk and predicted hazard is good, especially since no incidents were recorded during predicted low-hazard periods and the majority of incidents with the highest recorded risk (>66th percentile) are classified as high hazard.

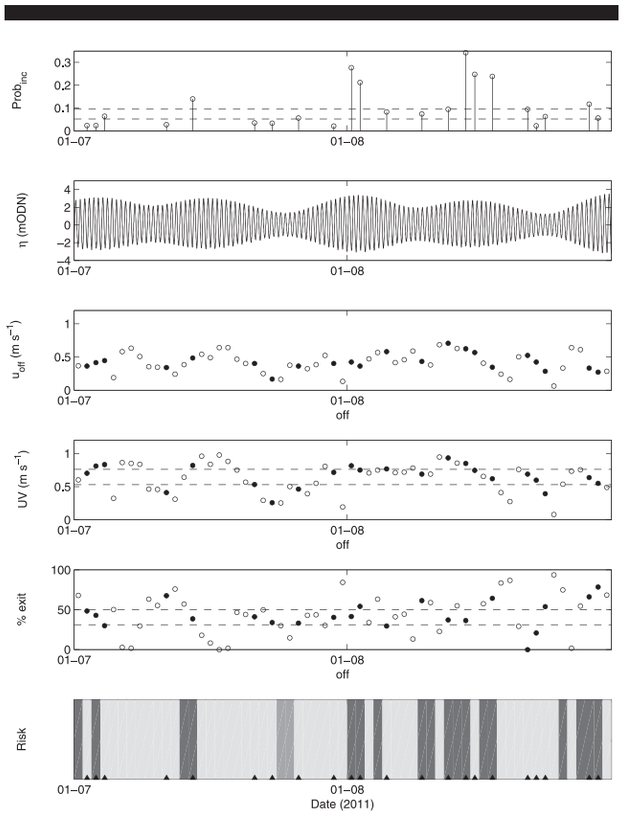

Figure 14. Comparison of hindcast model predictions with recorded RNLI incidents. (Top to bottom) Recorded risk of rip incident, $Prob_{inc}$, showing the 33rd and 66th percentiles (dashed lines); tidal elevation, η; maximum offshore-directed flow velocity, u_{off}; maximum rip speed, *UV*; percentage of drifters exiting the surf zone, %exit; and rip risk classification (color). Horizontal dashed lines indicate the hazard thresholds from Table 3, and solid markers and triangles indicate the occurrence of incident. (Color for this figure is only available in the online version of this paper.)

Table 3. *Allocation of rip current hazard.*

UV (m s^{-1})		% Exit	
Threshold	Score	Threshold	Score
<0.53	0.5	<0.31	0.5
0.53–0.76	1	0.31–0.5	1
>0.76	1.5	>0.5	1.5

Further Model Developments

One of the key issues for predicting rip current risk following the present modeling approach is the requirement for high-quality representative bathymetry. To date, our approach has used measured bathymetry collected with a sonar-equipped jet-ski with an approximate survey frequency of 4–6 weeks. It is difficult to measure bathymetry at a higher frequency given the obvious dependence on good weather and sea state; therefore, periods of rapid morphological change leading to changes in bar/rip orientation may be aliased over successive surveys. Furthermore, over longer timescales, the financial implications of ongoing surveys must be considered. In the future, we will explore implementation of a data model assimilation approach to minimize the required number of surveys.

Beach Wizard is a data model assimilation method whereby the nearshore subtidal bathymetry can be accurately estimated on the basis of video-derived observations of wave roller energy dissipation or video/radar-derived wave celerity (Sasso, 2012; van Dongeren *et al.*, 2008). The roller dissipation is quantified largely following the method of Aarninkhof *et al.* (2005), which assumes that, when scaled with the incoming wave energy flux, video image pixel intensity is a proxy for wave roller dissipation. For the present application, the time exposure video images collected by the Perranporth ARGUS station are scaled using the spectral output of the SWAN RWM. From an operational perspective, it is envisaged that Beach Wizard will be used to provide a weekly estimate of the bathymetry to use as input to the XBeach RRPM. Initial tests with an updated version of the Beach Wizard code have demonstrated that the use of Beach Wizard is a significant improvement over the use of outdated bathymetries and assuming no morphological change. When Beach Wizard–derived bathymetries are coupled with the RRPM, the prediction of rip current location, time of activation, and strength are good (Sasso, 2012). Wilson *et al.* (2010) introduce an alternative data assimilation approach whereby pressure and current data are assimilated into a 2D-H nearshore model. However, this requires the deployment of *in situ* surf zone instrumentation, so it is not applicable as a long-term operational tool.

An alternative approach is to use generic morphological templates, which are representative of the observed morphological types, without exactly reproducing the finer detail of the bathymetry (*e.g.*, Voulgaris, Kumar, and Warner, 2011). The implementation of this method into an operational rip risk prediction tool would require two steps: (1) the identification of the key morphological forms observed on the beach from the measured field data and (2) the allocation of the appropriate template to the morphology present on the beach at the time in question. The key drawback with this method is that, although it might be possible to predict the rip speed with some degree of confidence, the spatial location and phasing of the rips is unlikely to be reproduced because of the migration and elevation changes of the bars and rip channels.

Dissemination of Risk Information

The appropriate dissemination of rip risk information to the end user is a vital aspect of this tool. The initial questions that must be considered are: who is it most appropriate to inform of rip hazard levels and, secondly, what is the most suitable medium for achieving it? For this application, we have a hazard that varies in both the temporal and spatial domains but which also requires some basic understanding of the area under investigation and the necessary steps to mitigate exposure to the hazard (risk).

The senior beach lifeguards at the site in question are considered the most appropriate end users of an operational rip prediction tool because they possess the local site knowledge and basic understanding of rip currents to both interpret the outputs and make operational decisions concerning resource deployment. For the ease of knowledge transfer, it is likely that

an interactive web-based display, which enables the output to be customized between maps and time series to maximize the spatial and temporal evolution of the rip current hazard, is most appropriate.

CONCLUSION

Field data and beach incident statistics collected from a macrotidal beach in the southwest U.K. have been used to calibrate and validate a suite of numerical models to develop a rip current risk prediction tool. Eulerian and Lagrangian data collected over 87 tidal cycles indicate that the rip currents are highly dynamic at a range of spatial and temporal scales. The morphology of the lower intertidal beachface controls the specific cross- and alongshore location of the rip currents, whereas variations in the pattern of wave dissipation caused by the tidal translation of the surf zone at spring-neap and semidiurnal frequencies are the key temporal controls. The variation in offshore wave conditions is of secondary importance. At this macrotidal beach site, the largest rip current speeds are typically observed during spring low-tide conditions and low to medium wave heights. Three key behaviors are observed for the Lagrangian drift pattern associated with the rip currents: rotation, alongshore, and exit. Rotation and exit behaviors are typically observed under moderate conditions, whereas large waves result in a wide saturated surf zone, closing the seaward end of the rip channels and forcing strong alongshore-directed currents and drifter trajectories.

An operational regional wave model, validated against an inshore buoy deployment, is used to provide spectral wave boundary conditions to a 2D-H nonstationary model for coupled wave propagation and flow to predict rip current speed and behavior in the surf zone. The model is calibrated using the measured Eulerian flow and water depth data collected across the surf zone, and the resultant nearshore circulation patterns are validated by comparing the behavior of measured and numerical surf zone drifters. The model was run over a 2-month period, and the flow speed and behavioral output from the model were combined to allocate a rip current hazard rating, which was compared with measured beach lifeguard incident statistics. Using simple current velocity and rip exit thresholds to allocate hazard ratings, 64% of recorded incidents occurred under predicted high-risk conditions and 36% during medium-risk conditions. The rip risk prediction model was subsequently run in forecast mode to provide an example of operational-type output.

A key requirement for an operational rip risk prediction tool in a dynamic macrotidal environment is representative bathymetry. We discuss further model developments whereby a data model assimilation method is to be integrated into the present system to estimate the nearshore subtidal bathymetry accurately from video-derived wave roller dissipation maps. This approach is favored over the use of generic morphological templates, which are unlikely to reproduce the temporal or spatial variability observed in the rip currents.

ACKNOWLEDGMENTS

We extend our thanks to our excellent field and technical team: Peter Ganderton, Anthony Thorpe, Claire Earlie, Ellie Woodward, Tim Poate, Robert McCall, Megan Sheriden, Ivan Burton, Richard Kenyon, Pedro Almeida, Hanna Richardson, Jak McCarroll, Kit Stokes, Barbara Proenca, Joana van Nieuwkoop, Ruth Stafford, Matt Hilton, Bruno Castelle, Nicolas Bruneau, Dano Roelvink, Ap van Dongeren, Leo Sembiring, Jack Puleo, Mark Davidson, Iain Fairley, Fran Sieck, Emily Beaumont, and Jon Miles. We also thank the RNLI, and in particular Dickon Berriman, for their assistance at Perranporth. Phil Maynard from the Perranporth Youth Hostels Association is also thanked for his ongoing assistance. This research was funded by the Natural Environment Research Council (NERC)–RNLI partnership grant NE/H004262/1: DRIBS. We thank the reviewers for their constructive comments, which improved the paper.

LITERATURE CITED

Aarninkhof, S.; Wijnberg, K.; Roelvink, D., and Reniers, A., 2005. 2DH-quantification of surf zone bathymetry from video. In: Sanchez-Arcilla, A. (ed.) *Coastal Dynamics 2005: State of the Practice*. Barcelona, Spain; ASCE 978-0-7844-0855, pp. 1–14.

Austin, M.J.; Scott, T.M.; Brown, J.; Brown, J.; MacMahan, J.; Masselink, G., and Russell, P.E., 2011. Temporal observations of rip current circulation on a macro-tidal beach. *Continental Shelf Research,* 30, 1149–1165.

Booij, N.; Ris, R.C., and Holthuijsen, L.H., 1999. A third-generation wave model for coastal regions 1. Model description and validation. *Journal of Geophysical Research*, 104(C4), 7649–7666.

Brander, R.W., 1999. Field observations on the morphodynamic evolution of a low-energy rip current system. *Marine Geology,* 157, 199–217.

Bruneau, N.; Castelle, B.; Bonneton, P.; Pedreros, R.; Almar, R.; Bonneton, N., and Bretel, P., 2009. Field observations of an evolving rip current on a meso-macrotidal well-developed inner bar and rip morphology. *Continental Shelf Research*, 29(14), 1650–1662.

Castelle, B.; Michallet, H.; Marieu, V.; Leckler, F.; Dubardier, B.; Lambert, A.; Berni, C.; Bonneton, P.; Barthélemy, E., and Bouchette, F., 2010. Laboratory experiment on rip current circulations over a moveable bed: Drifter measurements. *Journal of Geophysical Research*, 115, C12008, 17p, doi: 10.1029/2010JC006343.

Coastal Processes Research Group, 201X. South-west UK regional SWAN wave model output. http://www.coastalprocesses.org/SWAN_output.html (accessed May 2012).

CoSMoS (Coastal Storm Modelling System), 201X. Rip currents: Dutch coast. http://cosmos.deltares.nl/RipCurrentsNL/index.html (accessed May 2012).

Daly, C.; Roelink, D.; van Dongeren, A.; van Thiel de Vries, J., and McCall, R., 2012. Validation of an advective-deterministic approach to short wave breaking in a surf-beat model. *Coastal Engineering,* 60, 69–83.

Earlie, C.S., 2011. The Effects of Winds on Rip Currents and Nearshore Cell Circulation on a Macro-Tidal Veach, UK. Plymouth, U.K.: Plymouth University, Master's thesis, 32p.

Engle, J.; MacMahan, J.; Thieke, R.J.; Hanes, D.M., and Dean, R.G., 2002. Formulation of a rip current predictive index using rescue data. National Conference on Beach Preservation Technology (Biloxi, Mississippi, Florida Shore and Beach Preservation Association).

Holman, R.A. and Stanley, J., 2007. The history and technical capabilities of Argus. *Coastal Engineering*, 54(6–7), 477–491.

Kim, I.H.; Kim, I.C., and Lee, J.L., 2011. Rip current prediction system combined with a morphological change model. *In:* Furmanczyk, K. (ed.), *Proceedings 11th International Coastal Symposium*, Journal of Coastal Research, Special Issue No. 64, pp. 547–551.

Lushine, J.B., 1991. A study of rip current drownings and related weather factors. *National Weather Digest,* 16, 13–19.
MacMahan, J.H.; Brown, J., and Thornton, E.B., 2009. Low-cost handheld global positioning system for measuring surf-zone currents. *Journal of Coastal Research*, 25(3), 744–754.
MacMahan, J.H.; Reniers, A.J.H.M.; Thornton, E.B., and Stanton, T.P., 2004. Infragravity rip current pulsations. *Journal of Geophysical Research*, 109, C01033, doi: 10.1029/2003JC002068, pp. 1–9.
MacMahan, J.H.; Thornton, E.B., and Reniers, A.J.H.M., 2006. Rip current review. *Coastal Engineering*, 53(2–3), 191–208.
Masselink, G. and Short, A.D., 1993. The effect of tide range on beach morphodynamics and morphology: a conceptual model. *Journal of Coastal Research,* 9(3), 785–800.
McKenzie, P., 1958. Rip current systems. *Journal of Geology,* 66, 103–113.
Murray, S.P., 1975. Trajectories and speeds of wind-driven currents near the coast. *Journal of Physical Oceanography*, 5, 347–360.
Plant, N.G.; Holland, K.T., and Puleo, J.A., 2002. Analysis of the scale of errors in nearshore bathymetric data. *Marine Geology*, 191(1–2), 71–86.
Reniers, A.J.H.M.; MacMahan, J.H.; Thornton, E.B.; Stanton, T.P.; Henriquez, M.; Brown, J.W.; Brown, J.A., and Gallagher, E., 2009. Surf zone surface retention on a rip-channeled beach. *Journal of Geophysical Research*, 114, C10010, 12p, doi: 10.1029/2008JC005153.
Roelvink, D.; Reniers, A.; van Dongeren, A.; van Thiel de Vries, J.; McCall, R., and Lescinski, J., 2009. Modeling storm impacts on beaches, dunes and barrier islands. *Coastal Engineering*, 56(11–12), 1133–1152.
Sasso, R., 2012. Video-Based Near Shore Bathymetry Estimation for Rip Current Forecasting on a Macrotidal Beach. Delft, The Netherlands: TU Delft, Master's thesis, 153p.
Schmidt, W.E.; Woodward, B.T.; Millikan, K.S.; Guza, R.T.; Raubenheimer, B., and Elgar, S., 2003. A GPS-tracked surf zone drifter. *Journal of Atmospheric and Oceanic Technology*, 20(7), 1069–1075.
Scott, T.M.; Russell, P.E.; Masselink, G.; Austin, M.J.; Wills, S., and Wooler, A., 2011. Rip current hazards on large-tidal beaches in the United Kingdom. *In:* Leathman, S. and Fletemeyer, J. (eds.), *Rip Currents: Beach Safety, Physical Oceanography, and Wave Modeling*. New York: CRC Press, Taylor & Francis Group, pp. 225–243.
Short, A.D. and Hogan, C.L., 1994. Rip currents and beach hazards: their impact on public safety and implications for coastal management. *In:* Finkl, C.W. (ed.), *Coastal Hazards: Perception, Susceptibility and Mitigation*, Special Issue No. 12, pp. 197–209.
Song, D.S. and Bae, H.K., 2011. Observation and forecasting of rip current generation in Haeundae Beach, Korea Plan and Experiment. *In:* Furmanczyk, K. (ed.), *Proceedings 11th International Coastal Symposium*, Journal of Coastal Research, Special Issue No. 64, pp. 946–950.
Spydell, M.; Feddersen, F.; Guza, R.T., and Schmidt, W.E., 2007. Observing surf-zone dispersion with drifters. *Journal of Physical Oceanography*, 37(12), 2920–2939.
Tolman, H.L., 1997. *User Manual and System Documentation of WAVEWATCH-III*. Washington, DC: National Oceanic and Atmospheric Administration, 104p.
van Dongeren, A.V.; Plant, N.; Cohen, A.; Roelvink, D.; Haller, M.C., and Catalán, P., 2008. Beach wizard: nearshore bathymetry estimation through assimilation of model computations and remote observations. *Coastal Engineering*, 55(12), 1016–1027.
Verbeek, W., 2011. Rip current forecasting. http://www.muien.nl/en/prdction/133-ripcurrent-forecasting.html (accessed May 14, 2012).
Voulgaris, G.; Kumar, N., and Warner, J.C., 2011. Methodology for prediction of rip currents using a three-dimensional numerical, coupled, wave current model. *In:* Leatherman, S. and Fletemeyer, J. (eds.), *Rip Currents: Beach Safety, Physical Oceanography, and Wave Modeling*. Boca Raton, Florida: CRC Press, Taylor & Francis Group, pp. 87–106.
Wilson, G.W.; Özkan-Haller, H.T., and Holman, R.A., 2010. Data assimilation and bathymetric inversion in a two-dimensional horizontal surf zone model. Journal of Geophysical Research, 115(C12), 1–17.
Wright, L.D. and Short, A.D., 1984. Morphodynamic variability of surf zones and beaches: a synthesis. *Marine Geology,* 56, 93–118.

APPENDIX

Definition of error parameters.

Parameter	Formula*	Description
Correlation coefficient (R^2)	$\mathrm{Cov}(m, c)/\sigma_m\sigma_c$	$R^2 = 1$ means no scatter; tendency may still be wrong.
Scatter index (SCI)	$\mathrm{rms}_{(c-m)}/\max(\mathrm{rms}_m\lvert\langle m\rangle\rvert)$	This is a relative measure of the scatter between model and data. The error is normalized with the maximum of the RMS of the data and the absolute value of the mean of the data; this avoids strange results for data with small mean and large variability.
Relative bias (Rel. bias)	$\langle c - m\rangle/\max(\mathrm{rms}_m\lvert\langle m\rangle\rvert)$	This is a relative measure of the bias, normalized in the same way as the SCI. This parameter relates the variance of the difference between data and model to the variance of the data.

* m = measured, c = computed.